

# Spectroscopic Deprojection-Analysis of Chandra Data of the Galaxy Cluster 3C 129

H. Krawczynski<sup>1</sup>

## ABSTRACT

We report on spectroscopic imaging observations of the nearby ( $z=0.022$ ) galaxy cluster 3C 129 performed with the ACIS detector on board of the Chandra X-ray observatory. Applying a deprojection analysis which fully takes into account the spatially resolved X-ray energy spectra we investigate the radial variation of temperature and particle density of the Intracluster Medium (ICM). While earlier data indicated a weak cooling flow and a cool cluster core, the Chandra data suggests that the core is hotter than the rest of the cluster: at the center we infer  $7.9_{-2.4}^{+4.4}$  keV while the mean temperature of all the other ICM shells is  $5.1 \pm 0.3$  keV (all errors on 90% confidence level). Based on the radial entropy profile we discuss the evidence for shock heating of the ICM at the cluster center. We discuss the possibility to use imaging spectroscopy data of more regular clusters to extract maps of the gravitational dark matter potential.

*Subject headings:* galaxies: clusters: individual (3C 129) — cosmology: dark matter — X-rays: galaxies: clusters

## 1. Introduction

While observations with the ROSAT and ASCA X-ray telescopes revealed non-homogeneous temperature of the ICM for a number of clusters (see e.g. Honda et al. 1996), the large scale radial temperature structure remained uncertain due to ROSAT's limited spectral resolution and coverage, and ASCA's non-negligible energy dependent point spread function. Based on ASCA observations of 30 galaxy clusters, Markevitch et al. (1998) found evidence for a general temperature decline with distance from cluster center. However, independent ASCA studies of the same and other galaxy clusters did not confirm this result (e.g., White 2000, Kikuchi et al. 1999). The new X-ray observatories Chandra and XMM-Newton with broad energy coverage of 0.3-10 keV (Chandra) and 0.1-15 keV (XMM-Newton) and angular resolutions of 0.5 arcsec (Chandra) and 15 arcsec (XMM-Newton) make it now possible to assess spatially resolved ICM X-ray energy spectra with sufficiently broad energy coverage and excellent angular resolutions. First observations of temperature or metallicity variations have already been reported for a number of clusters, e.g. Coma (Arnaud et al. 2000), A 2142 (Markevitch et al. 2000), Hydra A (McNamara et al. 2000),

A 1795 (Tamura et al. 2001), Sérsic 159-03 (Kaasstra et al. 2001), and Abell 1835 (Schmidt et al. 2001). On theoretical grounds one expects that the formation of clusters gives rise to substantial temperature, entropy, and metallicity gradients. The interplay of gravitational collapse and heating by accretion shocks produces characteristic radial temperature and entropy profiles (e.g. Evrard 1990). Depending on when the ICM is enriched with metals, also radial metallicity gradients could be observed (Metzler & Evrard 1994). Furthermore, merger of major cluster components produce pronounced ICM non-uniformities, and hydro/N-body simulations predict that the gradients could be observed several  $10^9$  years after the onset of the merger event (Roettiger et al. 1996). The decay of these non-uniformities might be reduced by magnetic fields which organize the ICM into a filamentary structure and thereby substantially reduce the ICM's heat conductivity and particle diffusion (Eilek 1999, but see also Narayan & Medvedev 2001).

In this letter we describe Chandra observations of the nearby rich cluster of galaxies 3C 129. Due to its low galactic latitude ( $l=160^\circ.5$ ,  $b=0.3^\circ$ ) the cluster has not been studied intensively at optical wavelengths. Based on ROSAT, Einstein, and EXOSAT data, Leahy & Yin (2000) estimated a total 0.2-10 keV luminosity of  $2.7 \times 10^{44}$  ergs  $s^{-1}$ , a total ICM gas mass of  $3.6 \times 10^{13} M_\odot$ , and a total cluster

<sup>1</sup>Yale University, P.O. Box 208101, New Haven, CT 06520-8101, USA, email: krawczastro.yale.edu

mass of  $\sim 5 \times 10^{14} M_{\odot}$ . The cluster harbors two radio galaxies: the prototypical head-tail galaxy 3C 129, and the weaker FR I source 3C 129.1. The main emphasis of the Chandra observation had been a study of the pressure balance between the ICM and the radio plasma and this study will be presented elsewhere.

In this letter we present a “spectroscopic deprojection-analysis” of the Chandra data. The deprojection-approach has been the standard-technique to convert observed X-ray surface brightness profiles into temperature and particle density profiles (see Fabian 1994, and references therein). Lacking spatially resolved X-ray energy spectra, these studies used several assumptions, namely that the ICM had a certain geometry, that the ICM was in hydrostatic equilibrium, and that the dark matter gravitational potential could be described by a certain shape and depth, together with an ICM temperature and metal abundance estimate derived from a non-imaging X-ray observation. The spatially resolved energy spectra from the Chandra and XMM-Newton observatories now make it possible to directly derive the radial temperature, particle density and metallicity profiles based only on assumptions about the ICM geometry. A similar analysis has independently been developed by Allen et al. (2001).

The rest of this letter is organized as follows. After describing the data set in Sect. 2 and the spectroscopic deprojection-method in Sect. 3, we will present the results of the observations in Sect. 4, and discuss their implications in Sect. 5. In the following we use  $H_0 = 65 \text{ km s}^{-1} \text{ Mpc}^{-1}$  and  $q_0 = 0.5$ ; the cluster is thus a distance of 100 Mpc and 1 arcmin corresponds to 28.7 kpc.

## 2. Data Set and Data Preparation

We use two 3C 129 pointings, one 30 ksec pointing with the ACIS S CCDs taken on December 9th, 2000, and one 10 ksec pointing with the ACIS I CCDs taken on January 9th, 2001. We detect X-ray emission near the radio cores of the radio galaxies 3C 129 and 3C 129.1 and exclude the corresponding sky regions, as well as an additional point source in the south-east of the cluster center from the following analysis. The radio galaxy 3C 129 has a 15 arcmin long tail which covers a substantial fraction of the field of view of the first observation at radial distances from 10 arcmin to 25 arcmin from the cluster center. We exclude the corresponding sky region from the analysis.

The analysis is performed with the CIAO 2.1 software. We divide the  $8.4' \times 8.4'$  solid angle re-

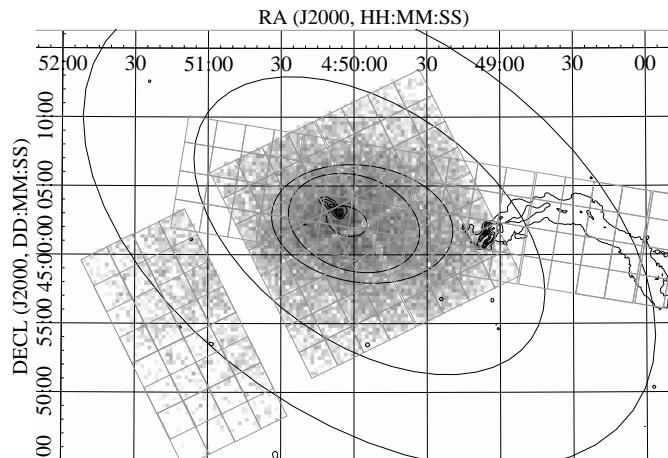


Fig. 1.— The ACIS I image (0.5-7.5 keV) with a  $32 \times 32$ -pixel binning. The 4 ellipses are shown which have been used to characterize the symmetry of the ICM’s surface brightness. The contour lines indicate the location of the radio galaxy 3C 129.1 at the cluster center and 3C 129 in the west of the cluster, and have been derived from 330 MHz VLA observations (Lane et al. 2001). The small rectangles cover the ACIS S and ACIS I field of views and show the sky-regions used for the deprojection analysis. The deprojection analysis uses only the regions with their centers within the outer ellipse.

gions of the sky covered by each ACIS chip in  $4 \times 4$  “analysis regions” of each  $126' \times 126'$  ( $256 \times 256$  pixels) solid angle coverage. This choice is a compromise between keeping the analysis feasible and using detector response functions which are as local as possible. We construct background data sets with the tool `make_acisbg` using the blank field background data sets of M. Markevitch. Only events in the energy range from 1.2 keV to 7.5 keV are used. We use a rather high lower threshold to minimize the influence of uncertainties in the detector response and in the contribution of the diffuse galactic X-ray emission. Above 7.5 keV the signal to noise ratio is poor. Application of the same requirements on the background rate as used for the production of the background data sets, reduces the exposure time of the first and second pointing to 19.5 ksec and 9.3 ksec, respectively. We use the tools `calcarf` and `calcrmf` of A. Vikhlinin to compute for each analysis region an Auxiliary Response File (ARF) and a Response Matrix File (RMF) averaged over the corresponding detector area. The analysis uses the ACIS S chips S2-S4, and the ACIS I chips I0-I4. Figure 1 shows the binned ACIS I picture together with the ACIS S and ACIS I fields of view, the analysis

regions, and the location of the two radio sources.

### 3. Spectroscopic Deprojection Analysis

The iso-brightness contours of 3C 129 show a slightly elliptical shape with the major axis along the east-west direction. Using the Chandra data together with the Einstein IPC contour map of (Leahy & Yin 2000), we define 4 ellipses with different centers and elasticities to parameterize the ICM surface brightness distribution at different distances from the cluster center (see Fig. 1). Assuming rotational symmetry around the major axis of each ellipse and using an interpolation scheme we define 11 approximately ellipsoidal ICM shells. For each shell  $s$  ( $s = 1, 2, \dots, 11$ ) we compute the volumes  $V(s, r)$  along the line of sight of the  $128 \times 128$  pixel analysis regions  $r$  ( $r = 1, 2, \dots, 95$ ) by simple numerical integration. For each shell we define one Raymond-Smith plasma model described by one set of parameters temperature,  $T(s)$ , particle density,  $N(s)$ , and metal abundances,  $A(s)$ . The algorithm works from shell to shell inwards, fitting the plasma parameters of the shell under consideration and using for the outer shells the best fit parameters determined before. The expression minimized by the fit algorithm for shell  $s$  (counting from the cluster center outwards) reads:

$$\chi^2(T(s), N(s), A(s); s) = \sum_{r' \in s} \sum_{I'} \left( C(r', I') - \frac{c(r')}{4\pi D_L^2} \sum_{s'=s}^{11} \int_0^\infty V(s', r') \times \kappa(N_H(r'); E') j_{\text{RM}}(T(s'), N(s'), A(s'); E') \times D_{r'}(I', E') dE' \right)^2 \quad (1)$$

The first sum of the right term runs over the regions  $r'$  which have their centers within the shell  $s$  under consideration; the second sum runs over the energy bins  $I'$  of each energy spectrum; in the third sum  $s'$  runs over the shell under consideration  $s$  and all outer shells.  $C(r', I')$  is the number of counts found in energy bin  $I'$  of region  $r'$ . The constants  $c(r') \approx 1$  allow for a slight deviation of the emissivity from the value expected from the assumed ellipsoidal geometry. We adjust these constants after fitting the flux normalization of a shell. The value  $D_L$  denotes the luminosity distance and  $\kappa$  and  $j_{\text{RM}}$  describe the photo-electric absorption and the emissivity of the Raymond-Smith plasma as function of photon energy  $E'$ , respectively. Finally,  $D_{r'}(I', E')$  is the detector response matrix

which gives the detection area times the probability with which an X-ray photon of energy  $E'$  will be reconstructed within the energy bin  $I'$  (averaged over the detector coordinates of region  $r'$ ). Due to the location of the cluster near the galactic plane we anticipated substantial variation of the neutral hydrogen column density across the field of view. We therefore performed radio observations with the Dominion Astrophysical Observatory to obtain  $N_{\text{H}}$ -values with arcminute resolution (principal investigator: T. Willis). Although the  $N_{\text{H}}$ -values change by 25% over the  $1.25^\circ \times 2.5^\circ$  field of view, the Chandra observations lie in a region of rather constant values of between  $0.84 \times 10^{22} \text{ cm}^{-2}$  and  $0.9 \times 10^{22} \text{ cm}^{-2}$ . We use in the following the  $N_{\text{H}}$ -values from the radio observations. Independent determination of the mean  $N_{\text{H}}$ -value from Chandra data gives consistent results. Note that our inferred hydrogen column densities deviate from those inferred by Leahy et al. (2000) ( $N_{\text{H}} = (0.57 \pm 0.03) \times 10^{22} \text{ cm}^{-2}$ ) from fitting the combined ROSAT and EXOSAT data with a one-temperature Raymond-Smith model. For each shell  $s$  we quote as radial distance  $R_s$  the mean distances of all analysis regions contributing to the plasma fit of this shell. We define the distance of a point from the cluster center as the half-diameter of the major axis of the associated ellipse.

Technically the deprojection-analysis is performed with the CIAO-tool `sherpa` running on a single script which contains all the information about the geometry of the shells and analysis regions. All errors are quoted on 90% confidence level. We estimate the increase of the statistical error on the parameters of the inner shells due to the statistical uncertainty of the fit-parameters of the outer shells with a simple Monte Carlo simulation and accordingly scale the errors on the fit-parameters. The uncertainty of the background normalization is estimated to be 10% (Vikhlinin et al. 2001). Determining the associated error in the parameters by repeating the full deprojection analysis with a background scaled up and down by 10%, we add these errors in quadrature to the statistical ones. The results of the outermost ICM shell depend on the assumed shell thickness. Since this is an inherent limitation of the deprojection method we do not show the fit results of the 11th ICM shell in the following. The fits give satisfactory  $\chi^2$ -values for 95 out of the 104 analysis regions. For 9 regions large  $\chi^2$ -values indicate a deviation of the plasma properties from the ellipsoidal shell or contamination by a field source, and we exclude these regions from the over-

all fit.

#### 4. Results

The Chandra image shows statistically significant evidence for X-ray emission out to 19 arcmin from the cluster core. We do not find evidence for abrupt changes in the ICM surface brightness, so we have no direct evidence for shocks or contact discontinuities.

Figure 2 shows the results of the deprojection analysis. Averaged over all shells, the mean cluster temperature is  $5.1 \pm 0.3$  keV. We have weak evidence for a hotter cluster core with  $k_B T = 7.9^{+4.4}_{-2.4}$  keV at  $R_1 = 1.4$  arcmin and a temperature decrease at the outermost 10th shell with  $k_B T = 3.5^{+1.2}_{-0.9}$  keV  $R_{10} = 18.1$  arcmin ( $k_B$  is the Boltzmann constant). Various estimates show that the low temperature of the outermost shell might be an artifact due to the soft diffuse galactic X-ray emission which begins to substantially contaminate the cluster emission at these distances from the cluster center. The dotted line of Fig. 2(a) shows the projected temperatures determined by fits of one component Raymond-Smith models. Naturally, the deprojected temperature varies more than the projected temperature which averages over several ICM shells.

The particle density (Fig. 2(b)) decreases monotonically from  $3.1 \times 10^{-3} \text{ cm}^{-2}$  at the cluster center to  $3.9 \times 10^{-4} \text{ cm}^{-3}$  at the cluster periphery. The errors on the metal abundances of individual ICM shells are rather large (typically about 0.4 solar abundances) and we do not show them here. The mean value averaged over all shells is  $0.2 \pm 0.1$  solar abundance. The thermal gas pressure, defined as  $p = N k_B T$  is shown in Fig. 2(c). The entropy per particle relative to the mean value of all shells  $s_0$  is shown in Fig. 2(d) and has been computed from  $s = \frac{3}{2} k_B \ln(T \rho^{-2/3}) - s_0$  with  $\rho \approx 0.6 m_P N$  and  $m_P$  the proton mass. The entropy profile will be discussed in more detail in the next section. Finally, the radiative cooling times are shown in Fig. 2(e). The cooling times have been computed according to  $t_{\text{cool}} = \frac{3}{2} N k_B T (\Lambda(N, T))^{-1}$  with the cooling function  $\Lambda$  which denotes the plasma emissivity including thermal bremsstrahlung and line emission processes (Sutherland & Dopita 1993). All radiative cooling times exceed the Hubble time, the shortest cooling time being  $30^{+20}_{-9}$  Gyr.

#### 5. Discussion

Based on a deprojection analysis of ROSAT surface brightness data Leahy & Yin (2000) inferred

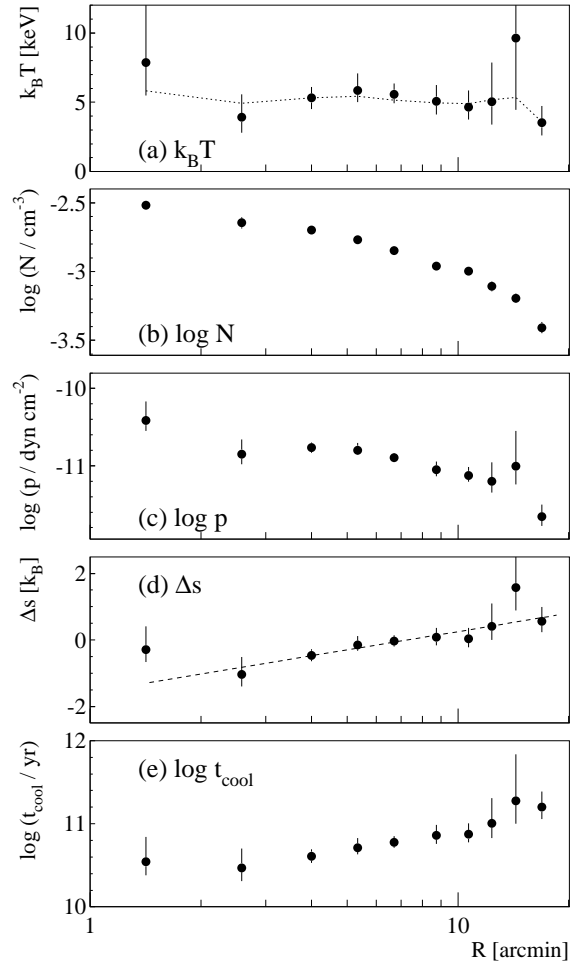


Fig. 2.— Results of the deprojection analysis showing from top to bottom: (a) temperature  $T$ , (b) particle density  $N$ , (c) gas pressure, (d) entropy, and (e) radiative cooling times. The dotted line in panel (a) shows the projected temperature, and the dashed line in panel (d) is for illustrative purposes only (see text).

a cluster temperature decreasing from  $\simeq 6$  keV at the cluster periphery (at  $\simeq 20$  arcmin from the cluster core) to about  $\simeq 3$  keV at the cluster center. The Chandra imaging spectroscopy data however, does not confirm this temperature decrease. On the contrary, both, the projected and deprojected temperature profiles indicate a hot cluster core. The discrepancy might be explained by one or more of the numerous assumptions entering the deprojection of surface brightness images mentioned in the introduction, as e.g. a true dark matter core radius substantially deviating from the assumed one.

A hot cluster core might be the result of shock heating. This possibility can be studied with the entropy per particle which is able to distinguish between ICM heating by adiabatic compression or by shocks. By definition, adiabatic compression does not increase the ICM entropy, while shock

heating, converting the energy of bulk plasma motion into heat, does increase it. A possible interpretation of the entropy profile is based on the dashed line in Fig. 2(d) which shows a fit to the entropy of the second to tenth shell and suggests that the entropy increases with distance from the cluster center. Indeed, in the framework of hierarchical clustering scenarios one expects that cluster formation through mass accretion produces a radially increasing ICM entropy as consequence of the growing strength of the cluster accretion shock as the total virialized cluster mass accumulates (see e.g. Tozzi et al. 2001, and references therein). The large entropy of the cluster core might be the result of shock heating by a jet or wind from the central radio galaxy 3C 129.1. The required power is modest:  $\simeq 10^{43} \frac{\Delta(k_B T)}{5 \text{ keV}} \frac{t_{3C129.1}}{100 \text{ Myr}} \text{ ergs s}^{-1}$  where  $\Delta(k_B T)$  is the temperature increase at the cluster center and  $t_{3C129.1}$  denotes the lifetime of the source. However, at the cluster center we do not find structure in the ICM surface brightness in direct support of this hypothesis.

The analysis presented here is plagued by large statistical and systematic errors. The first stem from the modest integration time and the low surface brightness of 3C 129. The latter mainly results from the asymmetric shape of the ICM and possible contribution of the diffuse galactic X-ray emission at larger cluster core distances. For brighter, more symmetric clusters the spectroscopic deprojection technique opens the possibility to determine the shape of the dark matter potential. The only uncertainties of such an analysis derive from the uncertain ICM geometry and from undetected ICM pressure components as kinetic pressure, magnetic field pressure and Cosmic Ray pressure.

*Acknowledgments:* The author would like to thank H. Völk and D. Harris for fruitful discussions on X-ray emission from galaxy cluster and AGN jets. W.M. Lane kindly provided the 330 MHz VLA map shown in Fig. 1, and T. Willis the  $N_H$ -data used for the deprojection analysis. Very helpful comments by an anonymous referee are gratefully acknowledged. This research has been supported by the NASA (NAS8-39073 and GO 0-1169X).

## REFERENCES

Allen, S.W., Etori S., Fabian A.C. 2001, MNRAS , 324, 877

Arnaud, M., Aghanim, N., Gastaud, R., et al. 2000, A&A, 365, L67

Edge, A.C., Stewart, G.C. 1991, MNRAS, 252, 414

Evrard, A.E. 1990, ApJ, 363, 349

Eilek, J. 1999, MPE Report 271, 71

Fabian, A. C. ARAA, 1994, 32, 277

Honda, H., et al. 1996, ApJ, 473, L71

Kaastra, J.S., Ferrigno, C., Tamura, T., et al. 2001, A&A, 365, L99

Kikuchi, K., Furusho, T., Ezawa, H., Yamasaki, N., Ohashi, T., Fukazawa, Y., Ikebe, Y. 1999, PASJ, 51, 301

Lane, W.M., Harris, D.E., Ensslin, T.A., Kassim, N.E., Perley, R.A. 2001, AAS, 199, 9814

Leahy, D.A., Yin, D. 2000, MNRAS, 313, 617

Markevitch, M., Forman, W.R., Sarazin, C.L., Vikhlinin, A. 1998, ApJ, 503, 77

Markevitch, M., Ponman, T.J., Nulsen, P.E., et al. 2000, ApJ, 541, 542

Metzler, C.A., Evrard, A.E. 1994, ApJ, 437, 564

McNamara, B.R., Wise, M., Nulsen, P.E.J., et al. 2000, ApJ, 534, L135

Narayan, R., Medvedev, M.V., ApJ, 562, L129

Roettiger, K., Burns, J.O., Loken, C. 1996, ApJ, 473, 651

Schmidt, R.W., Allen S.W., Fabian A.C. 2001, MNRAS, 327, 1057

Sutherland, R.S., Dopita, M.A. 1993, ApJS, 88, 235

Tamura, T., Kaastra, J.S., Peterson, J.R., et al. 2001, A&A, 365, L87

Tozzi, P., Norman, C. 2001, ApJ, 546, 63

Vikhlinin, A., Markevitch, M., Murray, S.S. 2001, ApJ, 551, 160

White, D. A. 2000, MNRAS, 312, 663